

Supporting Information for

Manufacture of Hydrophobic Nanocomposite Films with High Printability

Chunliang Zhang^{†, ‖}, Yapei Zhang^{†, ‖}, Ruitao Cha^{*, †}, Keying Long[†],

Juanjuan Li[†], and Xingyu Jiang^{*, †, ‡, §}

[†] Beijing Engineering Research Center for BioNanotechnology and CAS Key Lab for Biological Effects of Nanomaterials and Nanosafety, CAS Center for Excellence in Nanoscience, National Center for NanoScience and Technology, No. 11 Zhongguancun Beiyitiao, Haidian District, Beijing 100190, P. R. China.

[‡] Department of Biomedical Engineering, Southern University of Science and Technology, No. 1088 Xueyuan Road, Nanshan District, Shenzhen, Guangdong 518055, P. R. China.

[§] University of Chinese Academy of Sciences, 19 A Yuquan Road, Shijingshan District, Beijing 100049, P. R. China.

[‖] These authors contributed equally to this work.

* Corresponding Author:

E-mail: chart@nanoctr.cn (Ruitao Cha); Tel.: +86 10 82545631.

E-mail: jiang@sustech.edu.cn (Xingyu Jiang); Tel.: +86 10 82545620.

Pages: 13

Figures: 8

Table: 2

1. The characterization of NCC

The morphology of NCC was characterized by transmission electron microscope (TEM, HT7700, Hitachi, Japan). NCC dispersion (10 μL , 0.1% w/w) was dripped on Cu mesh. After dried at room temperature, the morphology of NCC was observed at accelerating voltage 120 kV after staining uranyl acetate.

Zeta potential of NCC dispersion (1 mL, 0.01 % w/w) was tested using a laser size instrument (Zetasizer Nano ZS, Malvern, UK).

XRD analysis of NCC was performed on an X-ray diffractometer (D/MAX-TTRIII (CBO), Japan) in the range of 2θ of 5° to 40° . Cu $K\alpha$ radiation and a maximum X-ray power of 40 kV and 30 mA were used. The crystallinity of NCC was determined by **Eq. (1)**:

$$\text{Crystallinity (\%)} = (I_{200} - I_{\text{am}}) / I_{200} \times 100\% \quad (1)$$

where I_{200} and I_{am} represent the peak intensity at $2\theta = 22.6^\circ$ and the intensity minimum between the (200) and (110) peaks ($2\theta = 18^\circ$), respectively.

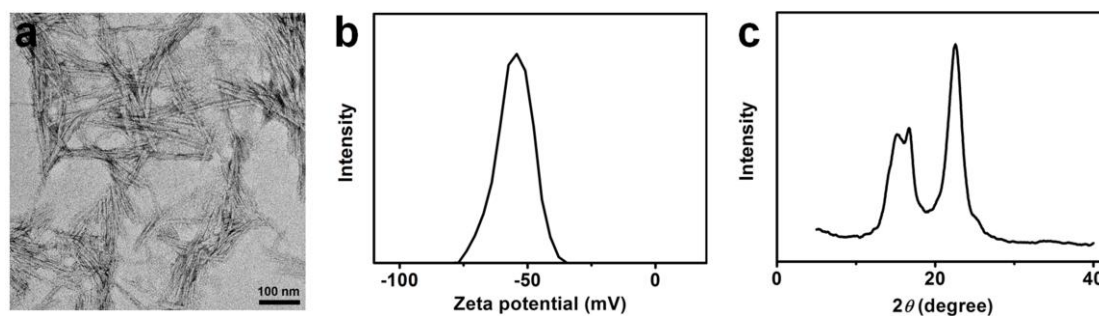


Figure S1. The characterization of NCC. a) The TEM image of NCC; b) The zeta potential of NCC; c) XRD spectrum of NCC.

2. The picture of the designed pattern

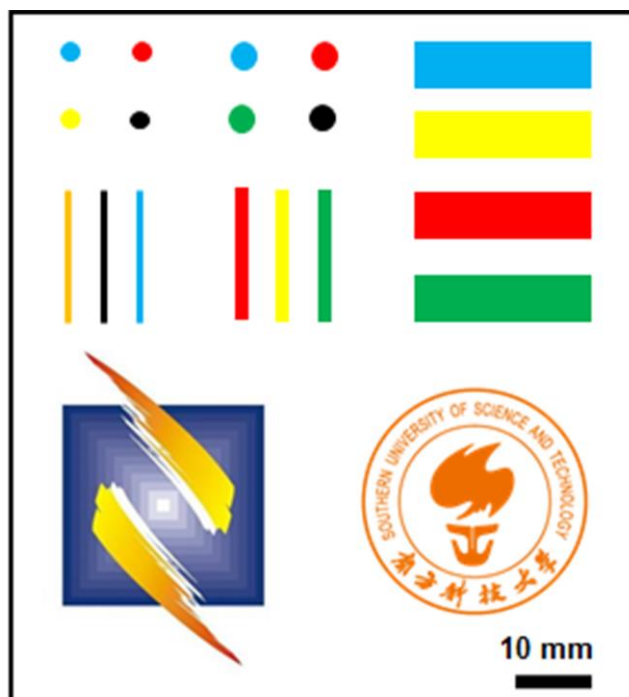


Figure S2. The picture of the designed pattern. The pattern composed of dots, lines and icons.

The dots with the colors of blue, red, yellow and black had the diameters of 2 mm and 3 mm. The horizontal lines with the colors of blue, yellow, red, black and green had the length of 21 mm, and the width of 6 mm. The vertical lines with the colors of orange, black, blue, red, yellow, and green had the length of 16 mm, and the width of 0.8 mm and 2 mm. The icons contained National Center for Nanoscience and Southern University of Science and Technology.

3. FTIR spectrums of GG and ASA

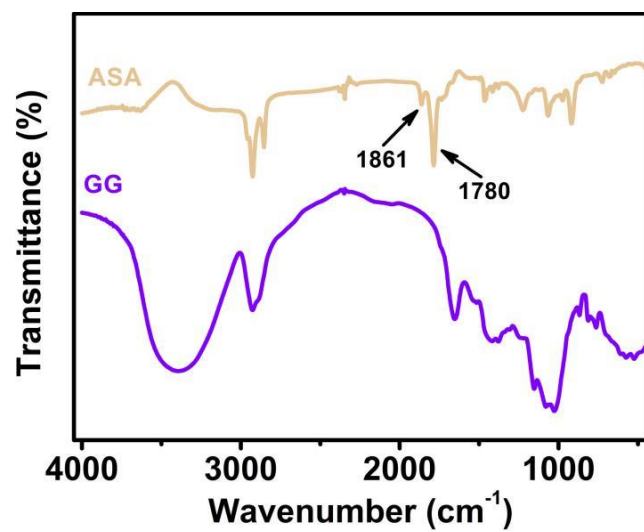


Figure S3. FTIR spectrums of GG and ASA.

4. The FTIR spectrums of nanocomposite films

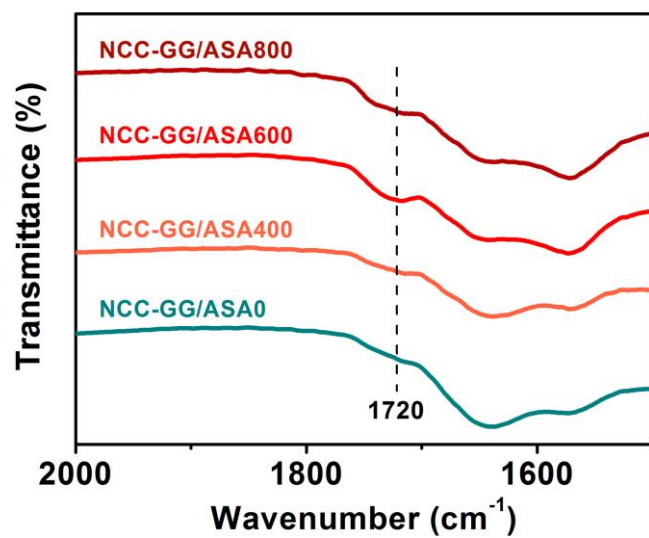


Figure S4. The FTIR spectrums of nanocomposite films.

5. The determination of the *DS* of ASA acylated GG

To determine optimal contents of ASA, different hydrophobic nanocomposite films were prepared. The coated contents of ASA were 200 ppm, 400 ppm, 600 ppm, 800 ppm, 1000 ppm, 1200 ppm, 1400 ppm, and 1600 ppm.

The *DS* of nanocomposite films was tested by the titration. Nanocomposite film (50 mg) and ethanol (15 mL, 75 %) were put in a beaker. After stirring for 30 min at room temperature, NaOH solution (15 mL, 0.5 M) was added and the mixture was heated at 75 °C for 15 min. HCl (0.1 M) was used to titrate excess NaOH and phenolphthalein was used as an indicator when the mixture was kept at room temperature after 12 h. Each group repeated three times. The *DS* was calculated by **Eq. (2)** and **Eq. (3)**:

$$DS (\%) = 162 \times B / (26600 - 266 \times B) \times 100\% \quad (2)$$

$$B = (M_{NaOH} \times V_{NaOH} - M_{HCl} \times V_{HCl}) \times 0.266 / m \quad (3)$$

where 162 and 266 represented the relative molecular weight of glucose unit and ASA, g/mol; M_{NaOH} and M_{HCl} represented the molar concentration of NaOH and HCl, mol·L⁻¹; V_{NaOH} and V_{HCl} represented the volume of NaOH and reacted the volume of HCl, mL; m represented the weight of nanocomposite films, g; B represented mass fraction of ASA in acetylated GG.

The reaction efficiency of ASA was calculated by **Eq. (4)**:

$$\text{Reaction efficiency (\%)} = (m / 162 \times DS) \times 266 / m_0 \times 100\% \quad (4)$$

where m_0 represented initial weight of ASA, g; m represented the weight of nanocomposite films, g.

When the coated content of ASA was lower than 800 ppm, the *DS* of ASA acylated GG significantly increased and the reaction efficiency of ASA had high value of larger than 95% (**Figure S4**). When the coated content of ASA was 800 ppm, the *DS* of ASA acylated GG was 1.3% and the reaction efficiency of ASA was 95.5%. High contents of ASA (larger than 800 ppm) had no obvious effect for the *DS* of ASA acylated GG, and significantly decreased the reaction efficiency of ASA. The optimum content of ASA was 800 ppm.

The content of esterified ASA on nanocomposite films can be calculated by the reaction efficiency of ASA (**Table S1**). When the coated content of ASA was lower than 800 ppm (such as 400 ppm, and 600 ppm), the contents of esterified ASA on nanocomposite films (such as 391 ppm, and 586 ppm) were similar to those of the coated contents of ASA. When the coated content of ASA was 800 ppm, the content of esterified ASA on nanocomposite films was 764 ppm. The high contents of ASA (larger than 800 ppm) decreased the contents of esterified ASA on nanocomposite films, which were due to the decrease of the reaction efficiency of ASA.

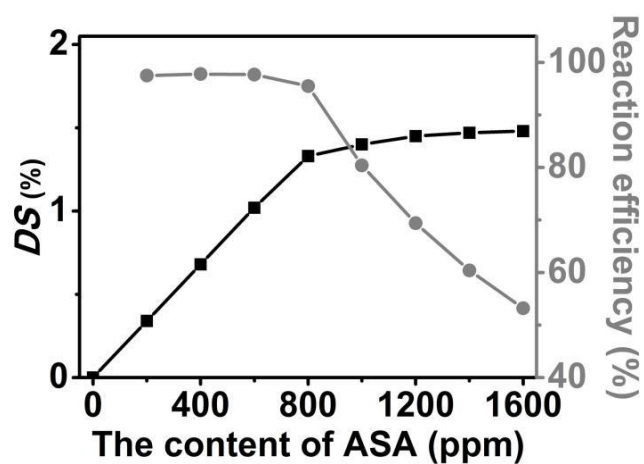


Figure S5. The *DS* of ASA acylated GG, and the reaction efficiency of ASA.

Table S1 The content of esterified ASA on nanocomposite films.

Nanocomposite films	Coated contents of ASA (ppm)	Content of esterified ASA (ppm)
NCC-GG/ASA200	200	195
NCC-GG/ASA400	400	391
NCC-GG/ASA500	500	489
NCC-GG/ASA600	600	586
NCC-GG/ASA700	700	676
NCC-GG/ASA800	800	764
NCC-GG/ASA1000	900	804
NCC-GG/ASA1200	1200	832
NCC-GG/ASA1400	1400	845
NCC-GG/ASA1600	1600	851

6. The gas permeability of nanocomposite films

The water vapor permeability (WVP) of nanocomposite films was calculated by

Eq. (5):

$$\text{WVP} = \text{WVTR} \times d / (SP \times \Delta\% \text{ RH}) \quad (5)$$

where d represented the thickness of films (μm); SP represented saturated pressure at at the test temperature (kPa); $\Delta\% \text{ RH}$ was the RH values difference within the chamber and the capsule (%).

The oxygen permeability (OP) of nanocomposite films was calculated by Eq.

(6):

$$\text{OP} = \text{OTR} \times d / \Delta P \quad (6)$$

where d represented the thickness of films (μm); ΔP represented oxygen partial pressure difference.

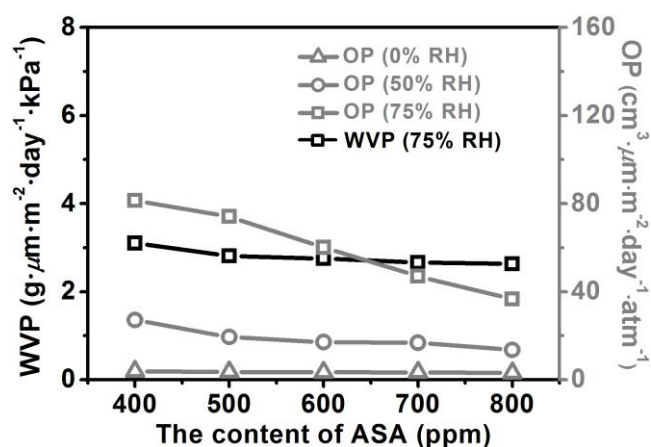


Figure S6. The effect of ASA on the water vapor permeability (WVP) at 75% RH, and oxygen permeability (OP) at 0% RH, 50% RH and 75% RH.

7. The cross-section morphologies of nanocomposite films

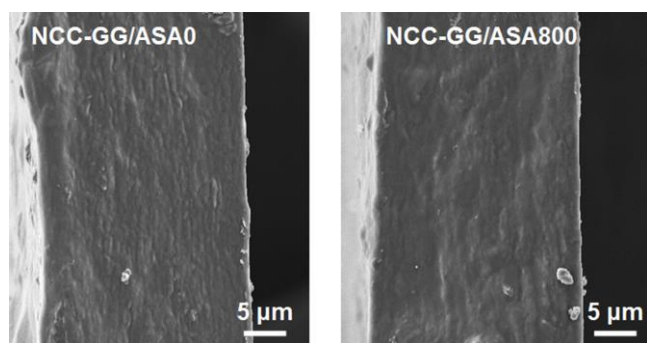


Figure S7. The cross-section morphologies of ASA-free nanocomposite films and NCC-GG/ASA800.

8. The physical properties of nanocomposite films

Table S2 The physical properties of nanocomposite films.

Nanocomposite films	Thickness (μm)	Density ($\text{g}\cdot\text{cm}^{-3}$)	Special tensile strength ($\text{kN}\cdot\text{m}\cdot\text{kg}^{-1}$)
NCC-GG/ASA0	24.63 ± 0.21	1.13	72.75 ± 0.63
NCC-GG/ASA400	24.68 ± 0.28	1.13	70.55 ± 0.38
NCC-GG/ASA500	24.73 ± 0.40	1.13	68.89 ± 1.13
NCC-GG/ASA600	24.77 ± 0.20	1.12	67.67 ± 1.01
NCC-GG/ASA700	24.82 ± 0.40	1.12	66.38 ± 0.76
NCC-GG/ASA800	24.90 ± 0.22	1.12	64.62 ± 1.01

9. The printability of polypropylene (PP) films and polyethylene terephthalate (PET) films

PP films were obtained from Decro Package Films Co., Ltd. PET films were purchased from Wantai Electronic Materials Co., Ltd. The designed pattern was printed on PP films and PET films by color laser printing. The patterns printed on PP film and PET film had the good color reproduction and had no diffused ink (**Figure S8a** and **S8b**).

Microscopic magnification images of ink dots on PP films and PET films were obtained (the magnified images of black ink dots showed in **Figure S8d** and **S8f**). After threshold processing, the thresholded images of ink dots were obtained (the thresholded images of black ink dots showed in **Figure S8e** and **S8g**). The value of dot roundness was almost the same for PP film and PET film, which were about 1.14 and 1.13 (**Figure S8c**). The proportions of black pixels of black ink dots on PP film and PET film were about 10.41% and 12.21%.

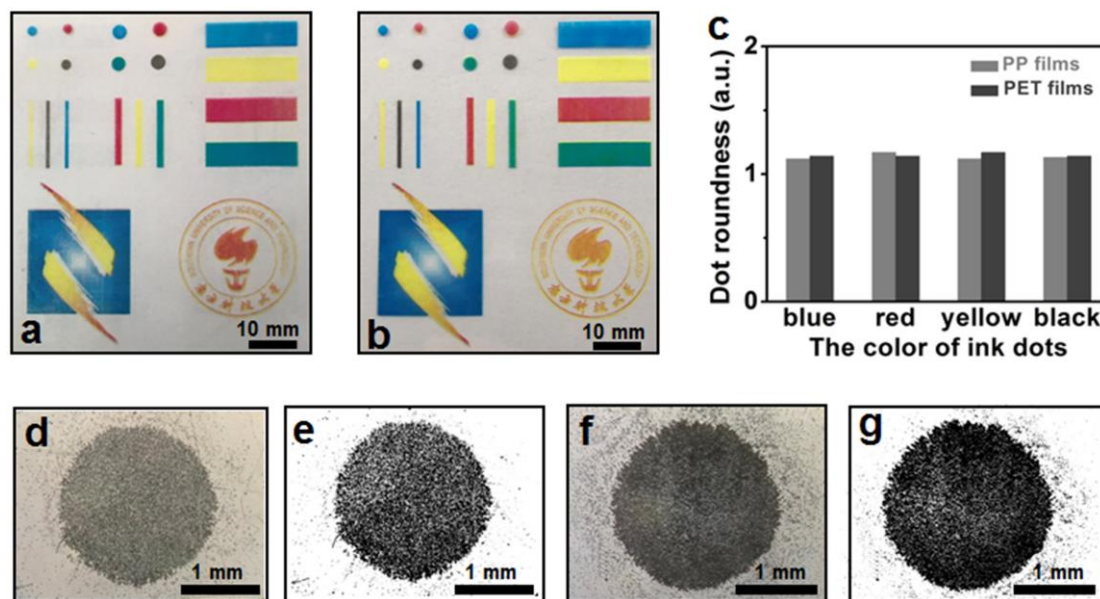


Figure S8 The printability of oil-based films by color laser printing. a) Pattern printed on PP films by color laser printing; b) Pattern printed on PET films by color laser printing; c) The dot roundness of ink dots with different colors printed on PP films and PET films; d) and f) Microscopic magnification images of black ink dots on PP films and PET films; e) and g) The thresholded images of black ink dots on PP films and PET films.